Magnetism in dense hexagonal iron

Gerd Steinle-Neumann*†, Lars Stixrude‡, and Ronald E. Cohen§

*Bayerisches Geoinstitut, University of Bayreuth, 95440 Bayreuth, Germany; ‡Department of Geological Sciences, University of Michigan, Ann Arbor, MI 48109; and §Geophysical Laboratory, Carnegie Institution of Washington, Washington, DC 20015-1305

The magnetic state of hexagonal close-packed iron has been the subject of debate for more than three decades. Although Mössbauer measurements find no evidence of the hyperfine splitting that can signal the presence of magnetic moments, density functional theory predicts an antiferromagnetic (afm) ground state. This discrepancy between theory and experiment is now particularly important because of recent experimental findings of anomalous splitting in the Raman spectra and the presence of superconductivity in hexagonal close-packed iron, which may be caused by magnetic correlations. Here, we report results from first principles calculations on the previously predicted theoretical collinear afm ground state that strongly support the presence of afm correlations in hexagonal close-packed iron. We show that anomalous splitting of the Raman mode can be explained by spin–phonon interactions. Moreover, we find that the calculated hyperfine field is very weak and would lead to hyperfine splitting below the resolution of Mössbauer experiments.

Physical properties of iron are of great importance to many fields in the sciences, as iron is one of the most abundant and stable elements in the universe and the very basis for the steel industry. Hexagonal close-packed (hcp) iron, the form stable at high pressure, plays a central role in geophysics, as the Earth's inner core is thought to be primarily composed of this phase (1, 2), and in our understanding of impact and explosive phenomena in iron and steel (3). The magnetic state of iron has a major influence on the physics of iron and iron alloys, including the relative stability of the iron polymorphs (4, 5). The magnetic structure of the hcp phase has been the subject of a scientific debate for three decades (6), leading to contradictory results from experiments and theory. Although experiments are interpreted to show the absence of magnetism in hcp iron (6–10), computations based on density functional theory find an antiferromagnetic (afm) ground state stable to $\approx$50 GPa (11), similar to magnetism in the double hcp phase (5). The possible presence of magnetism in hcp iron as further substantiated in this article has important implications. In geophysics many experiments are carried out on potentially magnetic hcp iron and are then extrapolated to pressures of Earth's core, into the nonmagnetic region of the hcp stability field at high pressure, and may consequently not be valid. The possible presence of magnetism in hcp iron also plays an important role in the discussion of the recently observed superconductivity of hcp iron (12, 13): Magnetic correlations in hcp iron appear to be necessary to explain the observed pressure dependence of its superconductivity (14–16).

The two lower-pressure polymorphs of iron are both magnetic. The phase stable around ambient conditions, body-centered cubic (bcc), owes its stability entirely to the presence of ferromagnetism (4). Heating above the Curie temperature causes the spins to disorder and the net magnetization to vanish, but the individual atomic moments are virtually unchanged in magnitude as temperature has little influence on the electronic structure. The face-centered cubic (fcc) phase is stable at higher temperatures at low pressure and has no ordered magnetic structure. However, local atomic moments are present in this phase; they interact antiferromagnetically and are responsible for anomalous phonon dispersion (17) and the antiinvar effect (18) in fcc iron. The fcc and hcp lattices are frustrated with respect to antiferromagnetism: it is impossible to surround every atom with atoms of opposite spin. Theory (19) and experimental studies of precipitates (20) reveal the fcc ground state to be an incommensurate spin wave.

Pressure has a large effect on the magnetic structure through the delicate balance between the potential energy, which stabilizes magnetism, and the kinetic energy, which stabilizes a nonmagnetic state. Potential energy is lowered by aligning spins since like spin electrons cannot occupy the same spatial orbital and therefore repel each other less than unlike spins. Lowering of the potential energy comes at the cost of higher kinetic energy as electrons of the same spin must occupy higher lying states. Magnetism tends to be favored in materials, such as bcc iron, with a high density of electronic states at the Fermi level (the highest occupied orbitals). Pressure broadens the electronic bands and tends to increase the separation between these states, causing the magnetic moments to decrease in magnitude on compression. Because the magnetization energy is more favorable at larger volumes, magnetism tends to expand the lattice and increase the compressibility as compared with the nonmagnetic state.

The absence of observable splitting in the Mössbauer signal in hcp iron to low temperatures (7, 8) places an upper limit of the hyperfine field (HFF) of only 5 kG (0.5 T) (8), leading to the conclusion that no significant magnetic moments are present. However, theoretical density functional theory methods give a stable afm state for hcp iron (11). This structure (afmII, Fig. 1) is characterized by alternating spin up and down planes perpendicular to the basal planes in the hcp cell, or a spin wave with wave vector $q = (0,1/2,0)$, at the high symmetry point M on the Brillouin zone boundary. The afmII phase has been predicted to be stable for hcp iron up to 60 GPa (Fig. 2), a finding that is robust within density functional theory computations using both the local density and generalized gradient approximation to the exchange correlation potential (11, 14, 15). Taking the afmII structure into account improves the agreement of computed and experimental equation of state for hcp iron significantly (11).

Recent experimental observations, including anomalous splitting of the Raman mode (21, 22), shed some light on the apparent discrepancy between theory and experiment. The Raman active phonon in a monatomic hcp system is the doubly degenerate transverse optic (TO or E_{2g}) mode. Consequently, only one peak is expected in Raman spectra of hcp iron. However, experiments using synthetic diamonds as anvils in the diamond anvil cell show two peaks up to pressures of 40 GPa (21, 22), suggesting a symmetry lower than the atomic arrangement. The afmII magnetic structure provides such a symmetry breaking mechanism, resulting in two TO modes, the B_{2g} and B_{3g} modes, characterized by displacements of the close-packed planes with respect to one another along the orthorhombic a-axis (TO_a) and b-axis (TO_b), respectively (Fig. 1). Both of these modes are Raman active.
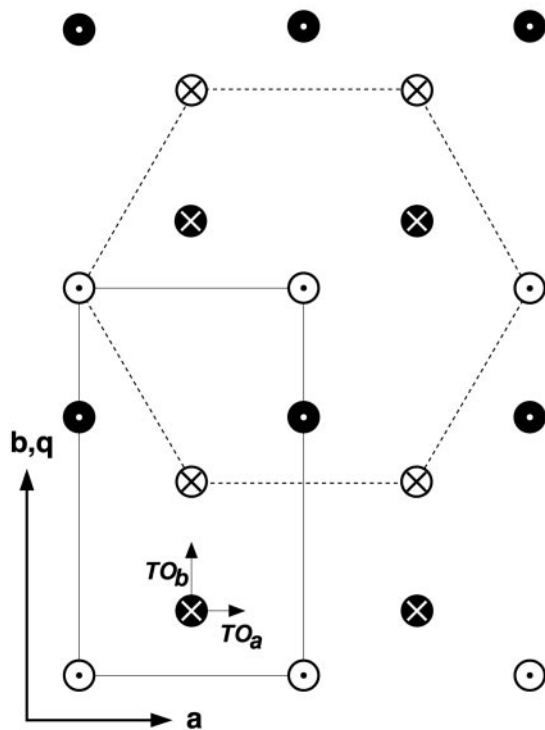

PHYSICS

Fig. 1. Orthorhombic afm ground state of hcp iron (afmII). Open circles show the atomic positions at $z = 1/4$, filled circles at $z = 3/4$ with arrows pointing in (crosses) and out of the plane (dots) indicating the direction of spin. The orthorhombic unit cell (space group Pmma) is given (solid lines, four atoms in the unit cell), and the axes are labeled. The direction of the wave vector q for the afmII spin wave is along the b axis, with length 1/2, at the M point on the Brillouin zone boundary ($q = 0,1/2,0$). The a- and b-axes define the eigenvectors for the TO modes (TO_a or B_{2g} and TO_b or B_{3g}). The c-axis is out of the plane. For reference, a hexagonal base at $z = 1/4$ is outlined (dashed lines).

Here, we calculate the TO mode frequencies and the HFF of the afmII structure over the compression range where finite afm moments are predicted (Fig. 2) by using the spin-polarized fully relativistic all-electron linearized-augmented plane-wave method (23, 24) with the generalized gradient approximation (25). Raman frequencies are calculated by the frozen phonon method: energy changes are evaluated in response to small displacements along the phonon eigenvector, with the second-order term yielding the frequency. For comparison we also calculate the TO mode frequency for the nonmagnetic structure. The HFF is computed self-consistently from the spin up and down charge density at the nucleus averaged about the Thompson sphere, generalizing the Fermi contact interaction to the relativistic case (26). To efficiently perform the calculations we fix the axial ratio $c/a = 1.6$ close to the experimentally (27) and computationally (11) determined equilibrium value.

Inspection of the magnetic structure reveals that fundamentally different spin interactions are involved in the two TO modes (Fig. 1). For the TO_a mode atoms approach nearest neighbors with unlike spin, corresponding to afm correlations. For TO_b atoms alternately move toward or away from a nearest neighbor with like spin, corresponding to ferromagnetic (fm) correlations. The resulting energy-displacement relations reflect the magnetic interactions (Fig. 3). For afm correlations the curvature of the energy is reduced with respect to the nonmagnetic case, and for fm correlations there is additional (along positive b) or reduced (negative b) repulsion. The calculated equilibrium magnetic moments are consistent with these findings (Fig. 3). The moment increases for displacements involving afm correlations (along a);
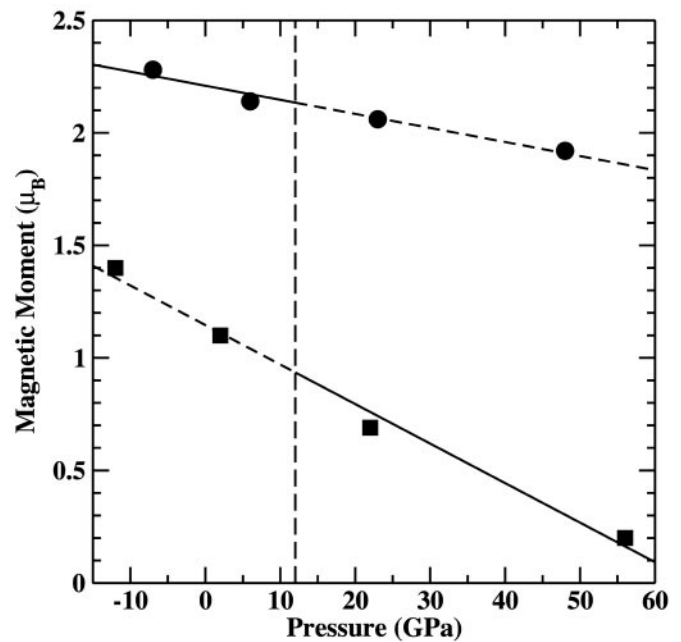

Fig. 2. Magnetic moments for iron as a function of pressure from theoretical results. Circles show the ferromagnetic moments for the bcc phase, and squares show spin-up afm moments (moments for both phases are taken within the muffin tin sphere) for the afmII phase of hcp iron. Units of the magnetic moments are the atomic units Bohr magneton (μ_B, 1 μ_B = 927.4·10^{-26} J/T). The vertical dashed line is the phase transition pressure from the bcc to the afmII phase, and magnetic moments in the stability regions of the two phases are shown by filled symbols. The lines through the bcc and afmII are linear interpolations to guide the eye.

for positive b they decrease considerably as like-spin nearest neighbors approach, and increase as this distance grows.

We find that the TO_a mode frequency agrees well with that of the lower-frequency, higher-amplitude peak found in the Raman experiments (21, 22) and that the TO_b mode frequency corresponds to the experimentally observed satellite peak at higher frequency (Fig. 4). The magnitude of the predicted TO mode splitting decreases as the afm moment is reduced by compression, in excellent agreement with the observation in the Raman experiments (Fig. 4). The systematic offset of the calculated frequencies by ≈ 20 cm^{-1} ($<10\%$) is typical for a comparison of computed and measured phonon frequencies (28). The magnitude of splitting predicted here is related to afmII, but other magnetic structures will also result in splitting of the TO mode.

Spin–phonon interactions have been found to have a strong effect on Raman scattering in a number of systems, including cupric oxide (29) and the copper-ruthenium oxide $RuSr_2GdCu_2O_8$ (30). The general character of the effect of spin–phonon interaction on the Raman spectra in these materials is consistent with the observations for hcp iron: broad, low amplitude, satellite peaks appear when the sample is below the Curie or Néel temperature.

The inherent frustration of the triangular lattice might lead one to suspect more complex spin arrangements than the one considered here, such as incommensurate spin waves or noncollinear structures, as in the case of fcc iron (19, 20), or a spin glass. If only nearest-neighbor afm interactions are important, the ground state of the hcp lattice is infinitely degenerate (31). Diep (31) showed further that in this case the hcp lattice adopts a collinear spin configuration at finite temperature, corresponding to the afmII structure, due to an entropic effect, known as ordering by disorder (32). Noncollinear calculations show that at least for high volumes the ground state is noncollinear, but
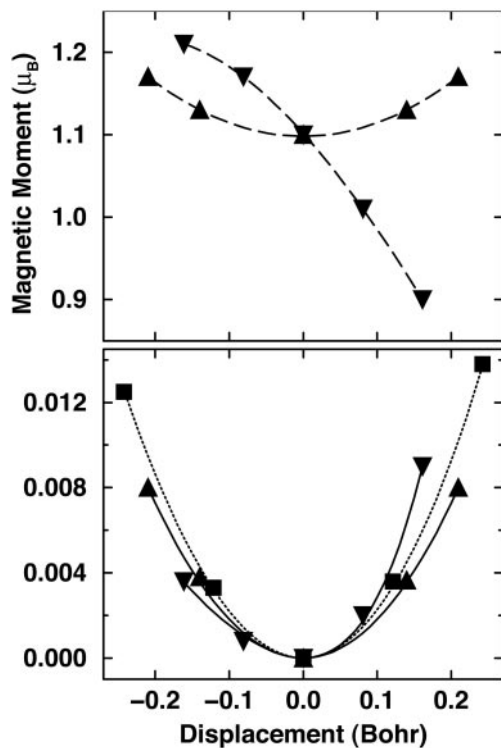
Fig. 3. (*Lower*) Energy of displacement of hcp iron at $V = 70$ Bohr^3 per atom. Relative energy changes (in Rydberg, the atomic unit of energy with 1 Ry = $2.179872 \cdot 10^{-18}$ J) as a function of displacement for the nonmagnetic structure (■), and the afmII structure for displacements along TO$_a$ (▲) and TO$_b$ (▼). Dotted and solid lines are third-order polynomial fits to the results. (*Upper*) The change in the afmII moment as a function of displacement for TO$_a$ and TO$_b$ (same symbols, with dashed lines to guide the eye).

Fig. 4. Raman frequencies as a function of atomic volume. The afmII structure results in two transverse optical frequencies with TO$_a$ being the lower (▲) and TO$_b$ (▼) the upper branch. Also shown are nonmagnetic calculations (■). The dashed lines through TO$_a$ and TO$_b$ are third-order polynomial fits in $V^{-2/3}$. Experiments (19, 22) identify two peaks in the Raman spectra up to 40 GPa in open symbols. The stronger peak is shown (△), and the weaker peak is shown (▽). The upper scale shows the corresponding pressure as based on the theoretical equation of state of the afmII structure (11). (*Inset*) Compared are the splitting in Raman frequencies from theory (▲) and experiment (△).

stabilization energies are small (33). One may consequently imagine a magnetic-phase transition sequence from a noncollinear ground state to the collinear afmII structure to a paramagnet with increasing temperature, which could also explain the strong decrease in amplitude and eventual disappearance of the satellite peak in experiments when the temperature is lowered (34). The absence of splitting in another set of experiments (35) can be explained by the use of natural diamonds for the cell anvils, where fluorescence significantly impairs the quality of the spectra, to the extent that the satellite peak would not be observable.

The inference of magnetism from the Raman splitting is in apparent conflict with the Mössbauer experiments that show no significant HFF for hcp iron: the disappearance of the typical Mössbauer sextet for ^{57}Fe at the transition from bcc to hcp iron has even been used to monitor the hysteresis and sharpness of this phase transition (9). To address the Mössbauer experiments we have calculated the HFF for afmII iron and find it to be only a few kG throughout its stability field (Table 1). This is two orders of magnitude smaller than the HFF for fm bcc iron. For bcc we find -323 kG at an atomic volume ($V = 80$ Bohr^3, with 1 Bohr = $0.529177 \cdot 10^{-10}$ m) close to the experimental zero pressure volume, in good agreement with the experimental saturation value (-339 kG), and obtain a slight decrease of the HHF as a function of compression (Table 1). The separation of the outermost peaks in the Mössbauer spectrum (L1 and L6) is diagnostic of the HFF, and a typical value of 4 kG for afmII would result in a separation of <0.2 mms^{-1}, within the width of the central Mössbauer peak. The small HFF for afmII results from the core and valence contributions having opposite signs and almost canceling (Table 1). It is worth noting that in the
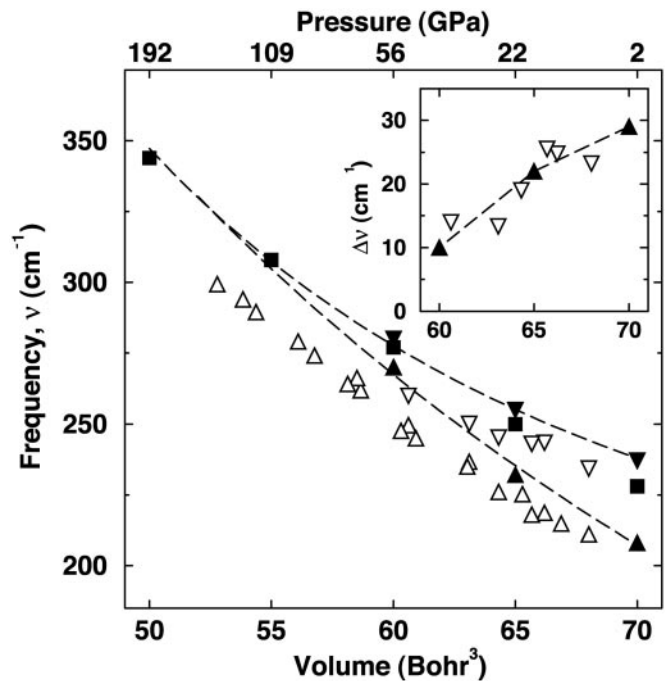
presence of an external field large internal magnetic fields develop in hcp iron (10); this anomalously large susceptibility supports our interpretation of hidden magnetic correlations in hcp iron.

Table 1. HFF in bcc and afmII hcp iron under compression

V, Bohr^3	P, GPa	M, μ_B	B, kG	B_c, kG	B_v, kG
bcc Fe					
79 (exp)	0	2.13	-339		
81 (ref. 40)		2.46	-316	-280	-36
80	-7	2.22 (2.28)	-329	-286	-43
75	6	2.14 (2.18)	-309	-279	-31
70	23	2.09 (2.06)	-287	-266	-21
65	48	1.90 (1.92)	-261	-249	-12
60	86	1.75 (1.77)	-226	-227	1
afmII Fe					
75	-12	0 (1.40)	3	-170	173
70	2	0 (1.10)	4	-132	136
65	22	0 (0.69)	4	-85	89
60	56	0 (0.20)	2	-31	33

Given are atomic volumes, V, the corresponding pressure, P, from the respective computational equation of state (11), and the magnetic moment, M, for the unit cell and inside the muffin tin sphere (in braces) in Bohr magnetons. The total HFF, B, and its contributions due to core, B_c, and valence electrons, B_v, follow. For the HFF computations we treat all electronic states up to $3s$ as core and higher lying states as valence electrons. For the afmII M in the muffin tin spheres and contributions to the HFF for the spin up atoms are given. A comparison to previous calculation (40) for bcc is included. We find that including spin-orbit coupling has negligible effect on the HFF. The calculations of the HFF were performed with the WIEN2K linearized-augmented plane-wave program (24).

Other experimental investigations of possible magnetic states in hcp iron have been inconclusive. Magnetism in hcp iron exists at overexpanded volumes in epitaxially grown multilayers on a ruthenium substrate (36). The change in nuclear x-ray absorption spectra across the bcc–hcp phase transition (37) results from a considerable reduction in magnetic moments across this transition, but cannot unambiguously be interpreted as absence of moments in the high-pressure polymorph. The change in absorption spectra is due to changes in the density of states and to spin-related satellites (38).

Long thought to be antithetical, superconductivity and magnetism are simultaneously observed in an increasing number of systems. Among these, $ZrZn_2$ is of particular interest: superconductivity and magnetism appear to be directly coupled as evidenced by the loss of superconductivity and magnetism at the same pressure (39). A similar connection between magnetism and superconductivity in hcp iron, which has been observed only recently (12, 13) has now been investigated. Although different in detail, computational studies (14–16) suggest that superconductivity in hcp iron is exotic and related to spin fluctuations. Jarlborg (14) in particular shows that the topology in pressure-temperature space and the critical temperature of superconductivity are determined by magnetic fluctuations.

Additional experiments investigating magnetism and magnetic correlations in iron under pressure and temperature, such as *in situ* susceptibility and neutron scattering, would be of great interest. They would not only elucidate the properties of this comment element, but help in understanding the equation of state for iron and shed important insight into extrapolations of physical properties to conditions of Earth's core. They will also help in understanding and refining theoretical methods for simulating and studying magnetism in materials.

1. Hemley, R. J. & Mao, H. K. (2001) *Int. Geol. Rev.* **43,** 1–30.
2. Vocadlo, L., Brodholt, J., Alfe, D., Gillan, D. & Price, G. D. (2000) *Phys. Earth Planet. Inter.* **117,** 123–137.
3. Millett, J. F. C., Bourne, N. K. & Rosenberg, Z. (1997) *J. Appl. Phys.* **81,** 2579–2583.
4. Bagno, P., Jepsen, O. & Gunnarsson, O. (1989) *Phys. Rev. B* **40,** 1997–2000.
5. Söderlind, P., Moriarty, J. A. & Wills, J. M. (1996) *Phys. Rev. B* **53,** 14063–14072.
6. Williamson, D. L., Bukshpan, S. & Ingalls, R. (1972) *Phys. Rev. B* **6,** 4194–4206.
7. Cort, G., Taylor, R. D. & Willis, J. O. (1982) *J. Appl. Phys.* **53,** 2064–2065.
8. Nasu, S., Sasaki, T., Kawakami, T., Tsutsui, T. & Endo, S. (2002) *J. Phys. Condens. Matter* **14,** 11167–11171.
9. Taylor, R. D., Pasternak, M. P. & Jeanloz, R. J. (1991) *J. Appl. Phys.* **69,** 6126–6128.
10. Taylor, R. D., Cort, G. & Willis, J. O. (1982) *J. Appl. Phys.* **53,** 8199–8201.
11. Steinle-Neumann, G., Stixrude, L. & Cohen, R. E. (1999) *Phys. Rev. B* **60,** 791–799.
12. Shimizu, K., Kimura, T., Furomoto, S., Takeda, K., Kontani, K., Onuki, Y. & Amaya, K. (2001) *Nature* **412,** 316–318.
13. Jaccard, D., Holmes, A. T., Behr, G., Inada, Y. & Onuki, Y. (2002) *Phys. Lett. A* **299,** 282–286.
14. Jarlborg, T. (2002) *Phys. Lett. A* **300,** 518–523.
15. Mazin, I. I., Papaconstantopoulos, D. A. & Mehl, M. J. (2002) *Phys. Rev. B* **65,** 100511 (R).
16. Bose, K. S., Dolgov, O. V., Jepsen, O. & Andersen, O. K. (2003) *Phys. Rev. B* **67,** 214518.
17. Zarestky, J. & Stassis, C. (1987) *Phys. Rev. B* **35,** 4500–4502.
18. Acet, M., Zähres, H., Wassermann, E. F. & Pepperhoff, W. (1994) *Phys. Rev. B* **49,** 6012–6017.
19. Uhl, M., Sandratskii, M. L. & Kübler, J. (1994) *Phys. Rev. B* **50,** 291–301.
20. Tsunoda, Y., Nishioka, Y. & Nicklow, R. M. (1993) *J. Magn. Magn. Mater.* **128,** 133–137.
21. Merkel, S., Goncharov, A. F., Mao, H.-K., Gillet, P. & Hemley, R. J. (2000) *Science* **288,** 1626–1629.
22. Goncharov, A. F., Gregoryanz, E., Struzhkin, V. V., Hemley, R. J., Mao, H. K., Boctor, N. & Huang, E. (2002) in *Proceedings of the International School of Physics "Enrico Fermi" CXLVII, "High-Pressure Phenomena,"* eds. Hemley, R. J., Bernasconi, M., Ulivi, L. & Chiarotti, G. (IOS, Washington, DC) pp. 297–316.
23. Singh, D. (1994) *Plane Waves, Pseudopotentials, and the LAPW Method* (Kluwer, Boston).
24. Blaha, P., Schwarz, K., Madsen, G. K. H., Kvasnicka, D. & Luitz, J. (2001) WIEN2K: *An Augmented Plane Wave + Local Orbitals Program for Calculating Crystal Properties* (Technische Universität Wien, Wien, Austria).
25. Perdew, J., Burke, K. & Ernzerhof, M. (1996) *Phys. Rev. Lett* **77,** 3865–3868; and correction (1996) **78,** 1396.
26. Blügel, S., Akai, H., Zellers, R. & Dederichs, P. H. (1987) *Phys. Rev. B* **35,** 3271–3283.
27. Jephcoat, A. P., Mao, H.-K. & Bell, P. M. (1986) *J. Geophys. Res.* **91,** 4677–4684.
28. Olijnyk, H., Jephcoat, A. P., Novikov, D. L. & Christensen, N. E. (2000) *Phys. Rev. B* **62,** 5508–5512.
29. Chen, X. K., Irwin, J. C. & Franck, J. P. (1995) *Phys. Rev. B* **52,** R13130–R13133.
30. Fainstein, A., Etchegoin, P., Trodahl, H. J. & Tallon, J. L. (2000) *Phys. Rev. B* **61,** 15468–15473.
31. Diep, H. T. (1992) *Phys. Rev. B* **45,** 2863–2867.
32. Henley, C. L. (1987) *J. Appl. Phys.* **61,** 3962–3964.
33. Thakor, V., Staunton, J. B., Poulter, J., Ostanin, S., Ginatempo, B. & Bruno, E. (2003) *Phys. Rev. B* **67,** 1804005 (R).
34. Goncharov, A. & Struzhkin, V. V. (2003) *J. Raman Spectrosc.* **34,** 532–548.
35. Olijnyk, H., Jephcoat, A. P. & Refson, K. (2001) *Europhys. Lett.* **53,** 504–510.
36. Saint-Lager, M. C., Raoux, D., Brunel, M., Piecuch, M., Elkaïm, E. & Lauriat, J. P. (1995) *Phys. Rev. B* **51,** 2446–2456.
37. Rueff, J. P., Krisch, M., Cai, Y. Q., Kaprolat, A., Hanfland, M., Lorenzen, M., Masciovecchio, C., Verbeni, R. & Sette, F. (1999) *Phys. Rev. B* **60,** 14510–14512.
38. Shirley, E. L. (1998) *Phys. Rev. Lett.* **80,** 794–797.
39. Pfleiderer, C., Uhlarz, M., Hayden, S. M., Vollmer, R., von Lohneysen, H., Bernhoeft, N. R. & Lonzarich, G. G. (2001*) Nature* **412,** 58–61; correction (2001) **412,** 660.
40. Battocletti, M., Ebert, H. & Akai, H. (1996) *Phys. Rev. B* **53,** 9776–9783.